

## Article

# Study on Bonding Behavior between High Toughness Resin Concrete with Steel Wire Mesh and Concrete

Qu Yu <sup>1,2</sup> , Yu Ren <sup>1,\*</sup> , Anhang Liu <sup>1</sup> and Yongqing Yang <sup>1,2</sup>

<sup>1</sup> School of Civil Engineering, Southwest Jiaotong University, Chengdu 610031, China; yuqu2014swjtu@163.com (Q.Y.); lah@my.swjtu.edu.cn (A.L.); yangyongqingx@163.com (Y.Y.)

<sup>2</sup> Sichuan Jiaoda Engineering Detection & Consulting Co., Ltd., Chengdu 610031, China

\* Correspondence: renyu@my.swjtu.edu.cn

**Abstract:** This paper investigates the interfacial bonding behavior between high toughness resin concrete with steel wire mesh (HTRCS) and concrete. A total of five sets of fifteen double shear specimens were tested for parameters including concrete strength and material properties of HTRCS composites. The test results showed that the failure mode of DS1 specimens was partial debonding and fracture, and the rest of the specimens were the fracture of HTRCS. The concrete strength and reinforcement ratios of HTRCS composites were positively correlated with interfacial adhesion properties. When the concrete strength was increased from C30 to C40 and C50, the ultimate load increased by 43.4% and 43.2%, respectively. The ultimate load capacity increased by 32.1%, with the reinforcement ratio of HTRCS composites increasing from 1.05% to 1.83%. Moreover, the bonding slip model and the bearing capacity formula for the interface between HTRCS composites and concrete were proposed, and the calculation values were in good agreement with the test values, with an average value of 0.978.

**Keywords:** high toughness resin concrete with steel wire mesh; concrete; interface bonding behavior; double shear test



**Citation:** Yu, Q.; Ren, Y.; Liu, A.; Yang, Y. Study on Bonding Behavior between High Toughness Resin Concrete with Steel Wire Mesh and Concrete. *Buildings* **2024**, *14*, 1341. <https://doi.org/10.3390/buildings14051341>

Academic Editor: Alberto Taliervo

Received: 7 April 2024

Revised: 4 May 2024

Accepted: 7 May 2024

Published: 9 May 2024



**Copyright:** © 2024 by the authors. Licensee MDPI, Basel, Switzerland. This article is an open access article distributed under the terms and conditions of the Creative Commons Attribution (CC BY) license (<https://creativecommons.org/licenses/by/4.0/>).

## 1. Introduction

Improving the normal performance and extending the service life of RC structures through simple and economical reinforcement measures is an inevitable requirement for the research and application of RC structures [1–3]. Traditional reinforcement methods include pasting fiber composite fabric [4], pasting steel plates [5], section enlargement methods [6,7], and using the NSM technique with steel bars or CFRP bars [8,9]. The pasting fiber composite reinforcement method considers the characteristics of lightweight and high strength FRP, and at the same time it has the advantage of low thickness of reinforcement; however, there are problems with the hollowing of the bonded interface, and the quality of the interface bond cannot be guaranteed [10]. The steel plate external bonding method has the advantage of convenient construction, but it has the problem that the steel plate cannot fit the concrete concave and convex surface well [5]. The section enlargement method can effectively enhance the structural stiffness and bearing capacity, but there are defects that increase the structural deadweight, prolong the construction period, and reduce the vertical clearance under the bridge [11]. The NSM technique embeds CFRP bars, steel bars, and adhesives into the grooves of the concrete members, but it requires extensive interface treatment [12]. In addition, fewer studies have been conducted on the effects that factors such as mandatory protective layer thickness and temperature variations have on it [13].

In recent years, the strengthening method of combining cement mortar and steel wire mesh has gradually gained the attention of scholars because of its convenient construction and excellent strengthening performance [14,15]. Marthong [16] used galvanized wire mesh mortar layers to reinforce concrete columns of different cross-sectional shapes and found that axial loads increased by 20% and 19% when circular and square columns were

reinforced with one turn of GSWM, respectively. Zhang et al. [17] investigated the flexural performance of reinforced concrete (RC) T-beams reinforced with HSSWM-PUC composites and found that the reinforced beams exhibited a 34% improvement with an increase in PUC thickness from 20 to 30 mm, and a 31.7% increase in ultimate and yield loads. However, this method is limited by the tensile properties of ordinary cement mortar, resulting in limited overall crack resistance of the reinforcement and premature failure of the reinforcement [18]. To solve the problem of early cracking of the reinforcement layer, related studies have proposed using engineering cementitious composites (ECCs) as binders and anchors [19]. With multicrock development and excellent ductility, ECC has shown it has a good effect on inhibiting cracks. However, ECC, as an inorganic material, has weak bonding and usually suffers from interfacial bond failure damage [20]. In addition, by drilling holes on the concrete surface, planting rebar and other methods can improve the bonding performance between the interface of ECC and concrete; however, there are also problems that affect its structural integrity and long construction period [21,22].

Due to the above reasons, this paper proposes high toughness resin concrete with steel wire mesh (HTRCS) composite material. High toughness epoxy resin concrete has the advantages of strong adhesion, high tensile strength, high toughness, high fluidity, and short curing time, which is conducive to rapid construction, shortening the reinforcement construction period [23]. Meanwhile, steel wire mesh embedded in the resin concrete enhances the strength of the composite material. Furthermore, the basis of the HTRCS composite reinforcement of RC members depends on whether HTRCS composite and RC matrix can work together, that is, the bonding behavior at the interface between HTRCS composite and concrete. Similar to other cement mortar composites for reinforcing RC structures, the bond strength of HTRCS composites is mainly related to the cross-sectional area of the wire mesh in the composite, the cross-sectional area of the resin concrete, and the strength of the concrete surface [24].

This paper investigates the interfacial bonding behavior between HTRCS composite material and concrete, which is investigated using a double shear test. Furthermore, the failure mode, force-displacement response, and strain of the specimens are analyzed. Moreover, we propose a bond-slip model and a bearing capacity formula for the interface between the HTRCS composite and the concrete.

## 2. Experimental Investigation

### 2.1. Details of the Specimens

To study the bond performance of HTRCS composite reinforced concrete members, double shear specimens were designed and fabricated to carry out interfacial bond tests. The dimensions of the specimens are shown in Figure 1. The test section was 300 mm × 150 mm × 150 mm, and the fixed section was 150 mm × 150 mm × 150 mm. The thickness of resin concrete was 20 mm and 40 mm, and the dimensions of steel wire mesh (transverse × longitudinal) were 13 mm × 25 mm, 15 mm × 25 mm, and 30 mm × 25 mm, respectively. The interfacial test section was bonded at a length of 300 mm and a width of 120 mm to ensure sufficient and effective bond length to observe strain transfer. The bond length of the fixed section was 150 mm, while the clip was used to apply pressure in the normal direction to enhance the interfacial bond. Before casting the HTRCS composite, the concrete interface needs to be cleaned to keep the interface clean.

A total of five types of specimens were designed for this test, and the main parameters were concrete strength and HTRCS material properties. Three specimens of each type were cast, and a total of fifteen double shear specimens were cast. For specimen numbers, “DS” represents the abbreviation “Double Shear”. DS1, DS2, and DS3 specimens were used to study the effect of concrete strength on bond performance. DS3 and DS4 specimens were used to study the effect of the cross-sectional area of the steel wire mesh on bond behavior when reinforcement ratios were approximately equal. DS4 and DS5 specimens mainly show the effect of reinforcement ratios in HTRCS on the bond behavior. The specimen parameters are shown in Table 1.

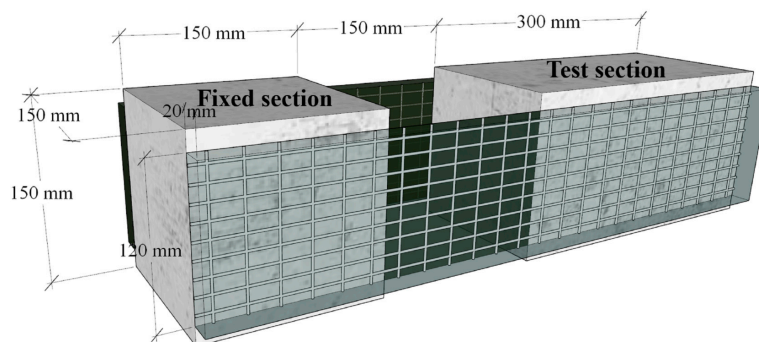


Figure 1. Dimensions of the specimens.

Table 1. Types of specimens.

Specimen	Concrete	Resin Concrete		Steel Wire Mesh			
		Thickness (mm)	Width (mm)	Diameter of Single Bar (mm)	Interval (mm)	$A_s$ (mm <sup>2</sup> )	$\rho$ /%
DS1	C30	20	120	2	13 × 25	28.3	1.18
DS2	C40	20		2	13 × 25	28.3	1.18
DS3	C50	20		2	13 × 25	28.3	1.18
DS4	C50	40		4	30 × 25	50.2	1.05
DS5	C50	40		4	15 × 25	87.9	1.83

Note:  $A_s$  is the cross-sectional area of the steel wire mesh,  $\rho$  is the reinforcement ratio of HTRCS.

## 2.2. Fabrication of the Specimens

Figure 2 shows the specimen fabrication process according to Chinese codes [25] with the following procedure:

- (1) Casting concrete: Standard molds were used to cast the concrete.
- (2) Preparing wire mesh: Trim the wire mesh to the required dimensions and paste the strain gauges according to Section 2.4.
- (3) Preparing molds: Wooden formwork was made, placing the test and fixed sections of concrete.
- (4) Casting resin concrete: Pouring resin concrete in wooden formwork.
- (5) Removing molds: After 24 h, remove the wooden formwork and remove the foam boards from the loading section.
- (6) Specimen curing: The fabricated double shear specimens were cured under standard conditions for 5 days.

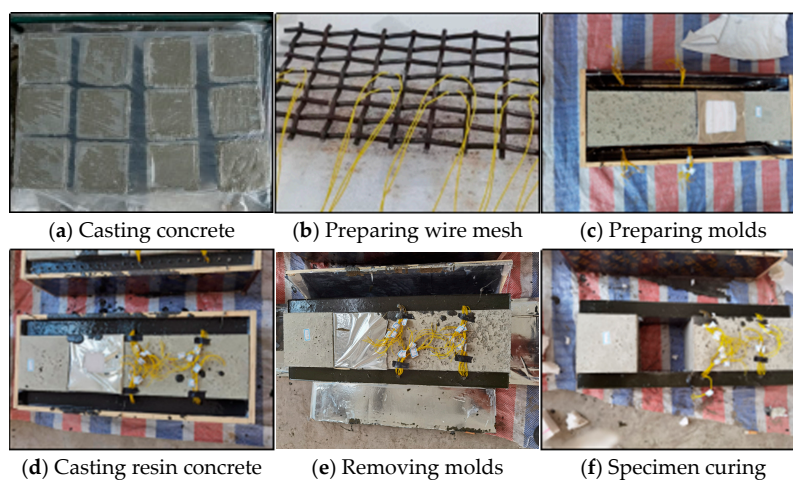


Figure 2. Fabrication of the specimens.

### 2.3. Materials Properties

The mix ratio of resin concrete used for the specimens [23] was resin colloid:hardener:continuous graded aggregate = 4:1.16:24.84. The material properties of resin concrete and ordinary concrete were measured according to Chinese codes [25]. The compressive strengths of C30, C40, and C50 ordinary concrete were measured to be 30.1, 42.3, and 54.6 MPa, and the tensile strengths were 2.35, 2.77, and 2.98 MPa, respectively. The tensile strength was 7.8 MPa, the modulus of elasticity was 12,500 MPa, and the compressive strength of resin concrete was 102.3 MPa [23], as shown in Table 2. The yield strength of steel wire mesh was 412 MPa.

**Table 2.** Properties of resin concrete.

Materials	Tensile Strength (MPa)	Elastic Modulus (MPa)	Compressive Strength (MPa)
Resin concrete	7.8	$1.25 \times 10^4$	102.3

### 2.4. Testing Procedure

The test setup used in this test is shown in Figure 3. The test setup consists of fixed, loading, and testing sections, in which the loading section includes load cells and hydraulic jacks. In the fixing section, normal pressure is applied using a clamp to improve the interfacial bond between the HTRCS composites and the concrete, thus ensuring that the damage occurs in the test section. In addition, the specimen should be kept parallel to the slide throughout the test to ensure that the specimen can slide freely with the rail. The loading level difference was about 1 kN, and the loading interval between two adjacent levels was about 3 s. When the displacement suddenly increased or the load increase rate slowed down, displacement-controlled loading was used, with a loading rate of 0.02 mm/s.

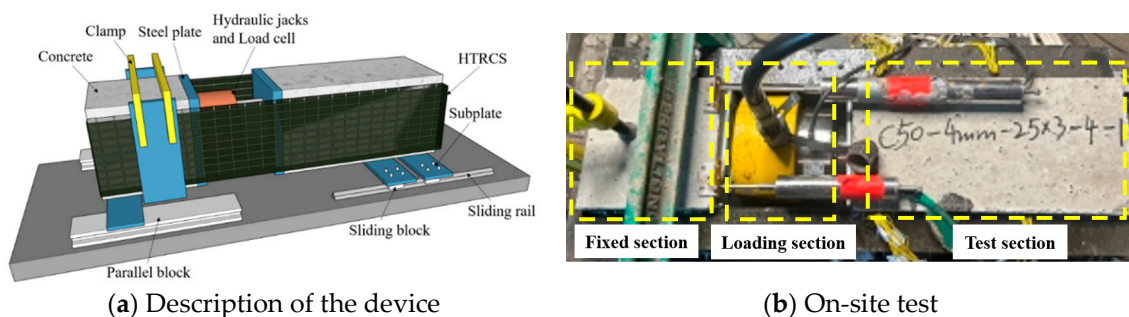


**Figure 3.** Test setup.

Figure 4 shows the arrangement of the strain measurement points of the wire mesh, and the specimen displacement measurement points. The first strain gauge, F1, is used to simulate the strain at the free end and is positioned in the middle of the loading section. Strain gauges F2–F8 are set on the test section to measure the strain in the test section. In addition, two Linear Variable Differential Transformers (LVDTs) were installed at the front of the test section to measure the relative displacement of the specimens.

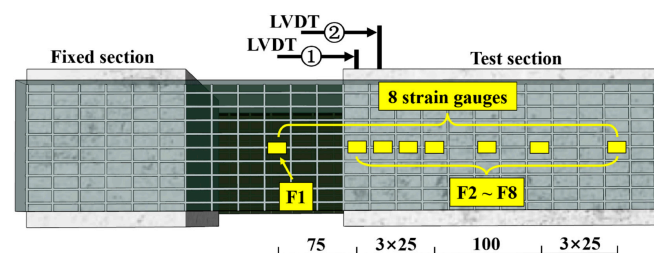


**Figure 4.** Measurement points.

### 3. Test Results

#### 3.1. Crack Patterns and Failure Modes

The failure modes of the double shear specimens are shown in Figure 5. Partial debonding and fracture of the HTRCS occurred in the DS1 specimen. The failure mode of the DS1 specimen was mainly due to the low interfacial bond between the HTRCS and the concrete when the concrete strength was low. At the same time, with the increase of load, the local stress concentration at the front end of the test section led to interfacial debonding and the subsequent fracture of the HTRCS material, as shown in Figure 5a. The fracture of the HTRCS in the loaded section occurred in the DS2, DS3, DS4, and DS5 double shear specimens, as shown in Figure 5b. This is because when the concrete strength increases, the interfacial bond strength increases, and therefore no interfacial debonding occurs. Meanwhile, the deformation of the HTRCS composites was less pronounced before the specimen fracture because the resin concrete in this study is a linear elastic material with an ultimate tensile strain of 0.000624. When the specimen was damaged, the resin concrete was pulled out and the wire mesh did not yield. A crisp sound was emitted at the time of destruction, and the failure process was rapid.

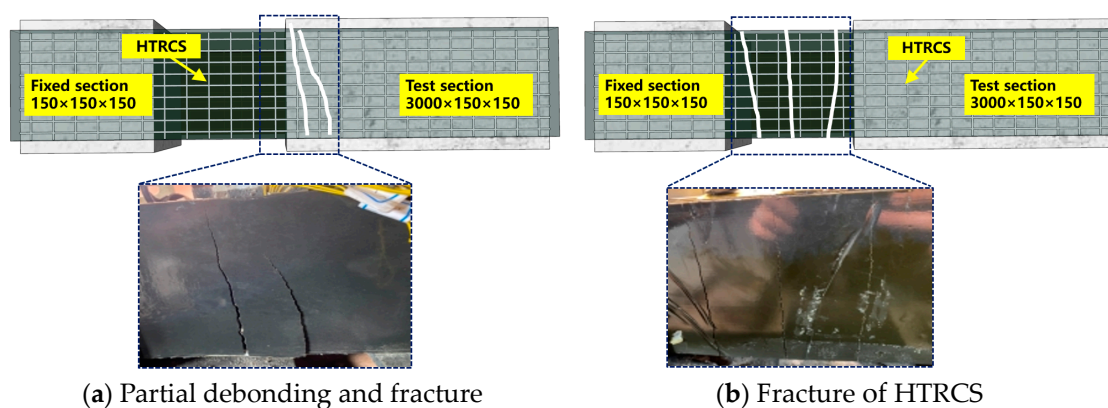


Figure 5. Failure modes.

The specimen extended interlayer cracks at the vertical cracks, as shown in Figure 6. Due to that, the resin concrete in the HTRCS composites pulled off when the specimen was damaged, and the resin concrete was squeezed by the wire mesh; thus, the interlayer cracks appeared. Furthermore, the bond between the wire mesh and the resin concrete was good during the whole test, and no significant slippage occurred.

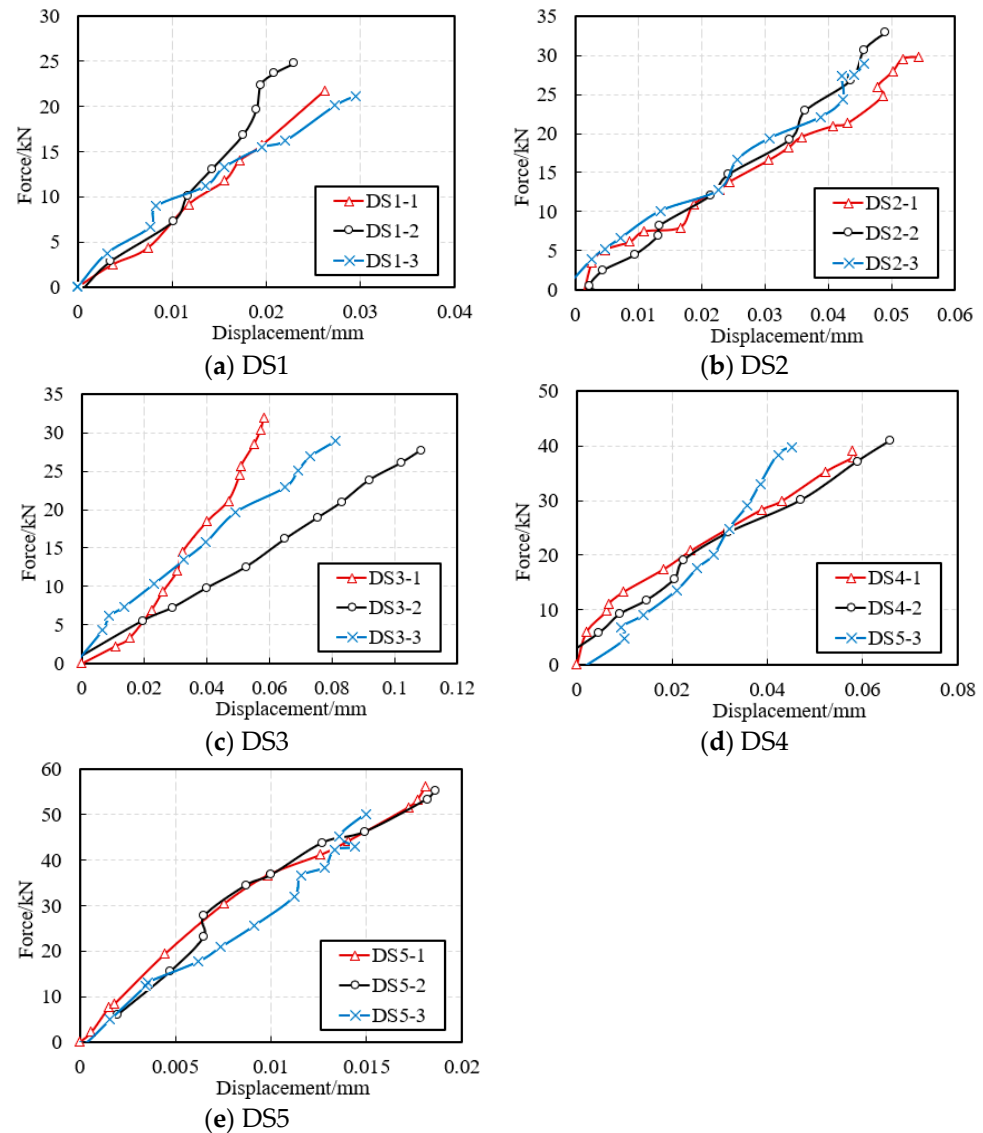


Figure 6. Interlayer cracks.

#### 3.2. Maximum Load and Displacement

Figure 7 shows the force-displacement curves of the double shear specimens. The results of maximum load  $P_{\max}$ , average maximum load  $\bar{P}_{\max}$ , displacement  $S$ , and average displacement  $\bar{S}$  of the specimens are shown in Table 3. The relationship between force and

displacement was basically linear for all specimens. This is due to the fact that the resin concrete in HTRCS composites is a linear elastic material, and the wire mesh did not yield when the resin concrete reached its ultimate strength. Therefore, HTRCS composites can be treated as linear elastic materials, the interfacial bonding is sufficient, and no interfacial peeling occurs, so the load-displacement curves are basically linear.



**Figure 7.** Force-displacement curves.

A comparison of the DS1, DS2, and DS3 specimens shows that the load carrying capacity is affected by the strength of the concrete. The ultimate loads of the DS2 and DS3 specimens are 43.4% and 43.2% higher than that of the DS1 specimen, respectively. This is because when the concrete is lower, the bond between HTRCS composites and concrete is weaker. After debonding at the front end of the test section, the partial HTRCS material fractured, so the bearing capacity of the DS1 specimen was lower. From specimens DS2 and DS3, it can be seen that their ultimate loads are basically the same. This is because when the concrete strength is increased, the interfacial bond is enhanced, and the ultimate load of the specimens is mainly related to the reinforcement ratio of HTRCS, which is the same for both groups of specimens.

**Table 3.** Maximum load and displacement.

Specimen	$P_{\max}$ (kN)	$\bar{P}_{\max}$ (kN)	$s/\text{mm}$	$\bar{S}$ (mm)	Failure Modes
DS1-1	21.18		0.026		Partial debonding and fracture
DS1-2	24.75	22.37	0.023	0.026	Partial debonding and fracture
DS1-3	21.16		0.029		Partial debonding and fracture
DS2-1	32.92		0.054		Fracture of HTRCS
DS2-2	32.31	32.07	0.048	0.049	Fracture of HTRCS
DS2-3	30.98		0.046		Fracture of HTRCS
DS3-1	32.05		0.061		Fracture of HTRCS
DS3-2	33.86	32.02	0.108	0.083	Fracture of HTRCS
DS3-3	30.16		0.081		Fracture of HTRCS
DS4-1	40.05		0.058		Fracture of HTRCS
DS4-2	42.14	40.69	0.066	0.056	Fracture of HTRCS
DS4-3	39.88		0.045		Fracture of HTRCS
DS5-1	56.89		0.018		Fracture of HTRCS
DS5-2	54.73	53.75	0.019	0.017	Fracture of HTRCS
DS5-3	49.64		0.015		Fracture of HTRCS

A comparison of the DS3 and DS4 specimens shows that the ultimate load of the specimens is positively correlated with the cross-sectional area of the reinforcement when the difference in the reinforcement ratio in the HTRCS composites is small. The ultimate load of the DS4 specimen is increased by 27.1% compared to the DS3 specimen. A comparison of the DS4 and DS5 specimens shows that when the cross-sectional area of resin concrete is determined, the reinforcement ratio of HTRCS composites is positively related to the ultimate load capacity of the specimens, and the ultimate load capacity increased by 32.1% with the reinforcement ratio of HTRCS composites increasing from 1.05% to 1.83%.

### 3.3. Strain-Distance Analysis

The strain distribution of the specimen is shown in Figure 8. Strain gauge F1 simulates the strain at the free end, with the distance of 0 mm in the test section. Strain gauges F2–F8 draw the strain distribution curve according to the actual distance from the end of the test section. Because the strain distribution curves of three specimens in each type are basically the same, one specimen in each group is selected for display.

The DS1 specimen was damaged when the strain reached  $400 \mu\epsilon$ , while the strains of the DS2 and DS3 specimens reached  $600 \mu\epsilon$ , which is close to the ultimate tensile strain of resin concrete. Meanwhile, the stress transfer distance is about 140 mm for the DS1 specimen and 190 mm for the DS2 and DS3 specimens. A comparison of the DS1, DS2, and DS3 specimens shows that as the strength of the concrete increases, the bonding effect between the interfaces is enhanced, the HTRCS composite is more fully utilized, and the strain transfer range is increased.

The strain transfer distance of the DS4 specimen is about 190 mm, and that of the DS5 specimen is about 260 mm. By comparing the DS4 and DS5 specimens, it can be seen that with the increase of the reinforcement rate in HTRCS, the strain transfer distance increases and the stress transfer effect is more significant.

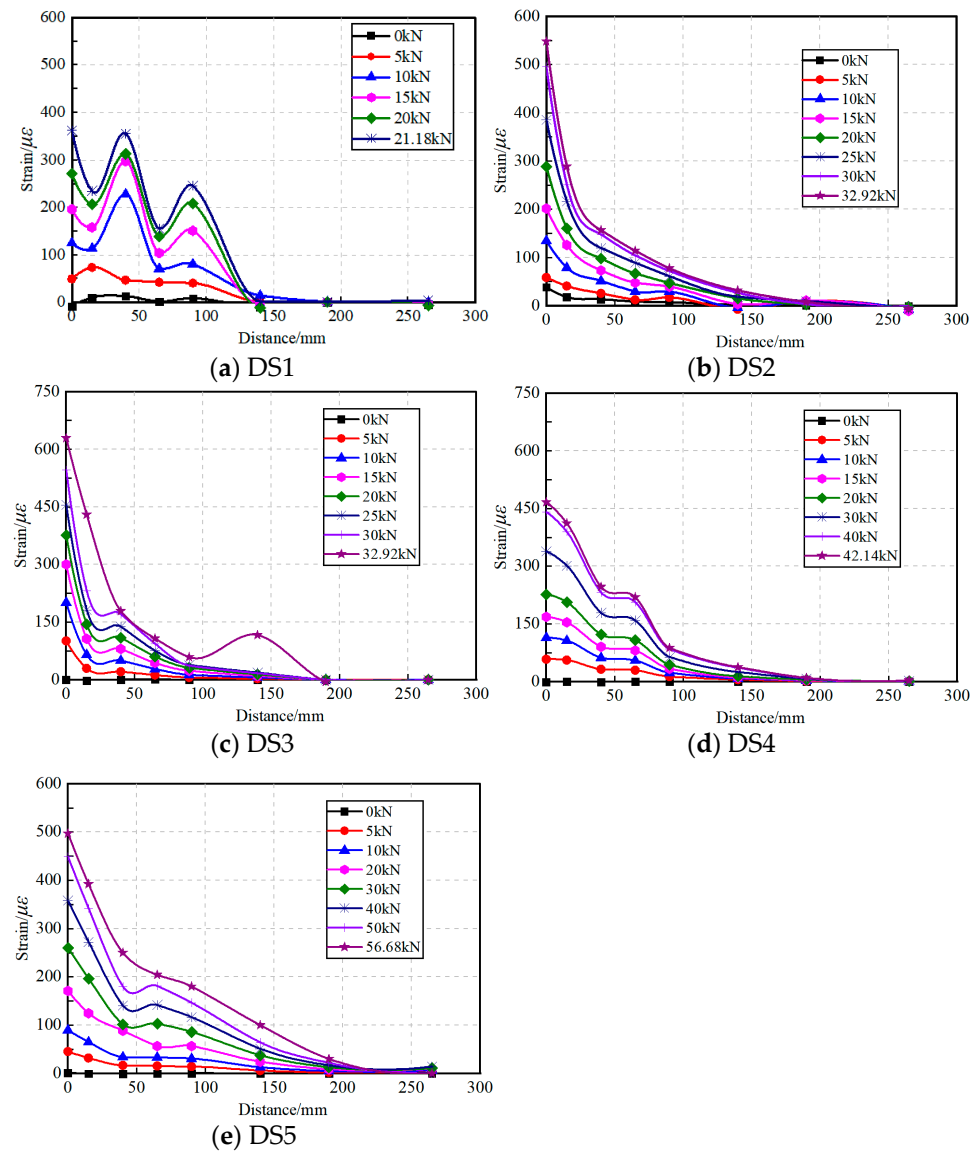


Figure 8. Strain distance curve.

## 4. Bond-Slip Model and Bearing Capacity Formula

### 4.1. Bond-Slip Model

In order to investigate the material properties of HTRCS composites and the effect of concrete strength on the bonding behavior at the interface between HTRCS composites and concrete, the local stress-slip curves need to be obtained first. The strain distance curves (Figure 8) from the double shear experiments were converted by the conversion formula proposed in [26], and the expressions are given as follows:

$$\tau_i = \frac{E_H t_H (\varepsilon_i - \varepsilon_{i-1})}{\Delta d} \quad (1)$$

$$S_i = \frac{\Delta d}{2} (\varepsilon_0 + 2 \sum_j^{i-1} \varepsilon_j - \varepsilon_i) \quad (2)$$

where  $\tau_i$  and  $S_i$  are the interfacial bonding stress and slip at strain gauge  $i$ ;  $\varepsilon_0$  is the strain at the free end, which is the strain of F1;  $\varepsilon_j$  ( $j = 1, \dots, i$ ) is the strain at strain gauge  $j$ ;  $E_H$  is the elastic modulus of the HTRCS composite;  $t_H$  is the thickness of the HTRCS composite; and  $\Delta d$  is the corresponding distance between each strain gauge.

In exploring the interfacial bonding behavior between HTRCS and concrete, we assumed that the deformation of resin concrete and steel wire mesh before specimen damage are the same. Therefore, the expressions for the ultimate stress and modulus of elasticity of HTRCS are as follows:

$$f_H = (f_{rc}A_{rc} + \varepsilon_{rc}E_sA_s)/A_H \quad (3)$$

$$E_H = (E_{rc}A_{rc} + E_sA_s)/A_H \quad (4)$$

where  $f_H$  is the tensile stress of the HTRCS;  $f_{rc}$  is the tensile strength of the resin concrete;  $A_H$ ,  $A_{rc}$ , and  $A_s$  are the cross-sectional area of the HTRCS, resin concrete, and steel wire mesh, respectively;  $E_{rc}$  and  $E_s$  are the elasticity moduli of the resin concrete and steel wire mesh, respectively;  $\varepsilon_{rc}$  is the tensile strain of the resin concrete; and  $\varepsilon_{rc} = 0.000624$ .

After plotting the local stress-slip curves, the local stress-slip relationship closer to the free end is selected for fitting the overall stress-slip curve. In addition, the stress-slip model is compared to the formulae presented in [27,28], in which the model shape is controlled by three parameters with the following expression:

$$\tau = \tau_{max} \frac{S}{S_0} \frac{n}{(n-1) + (S/S_0)^n} \quad (5)$$

where  $\tau_{max}$  is the maximum shear stress,  $S_0$  is the slip at peak, and  $n$  is the coefficient of the softening branch.

The fitting diagram of the interface bond-slip curve is shown in Figure 9. The fitting results are somewhat discrete, but basically reflect the bond-slip relationship at the interface. Similarly, bond-slip curves were plotted for all specimens, and the obtained curve control parameters,  $\tau_{max}$ ,  $S_0$ , the tensile strength of concrete ( $f_t$ ), and the elasticity modulus of the HTRCS ( $E_H$ ), are listed in Table 4. According to the experimental data, the softening coefficient  $n$  is uniformly taken as 3.6.

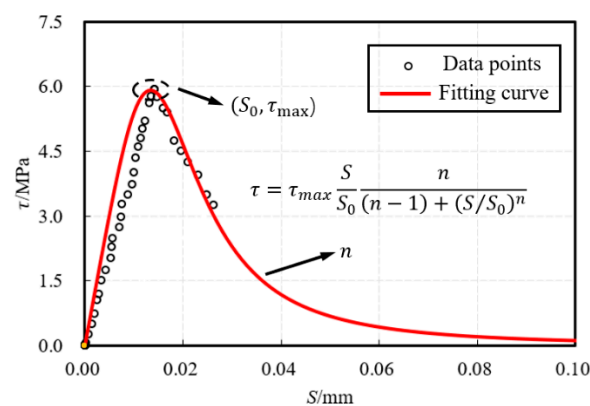


Figure 9. Interface bond-slip curve.

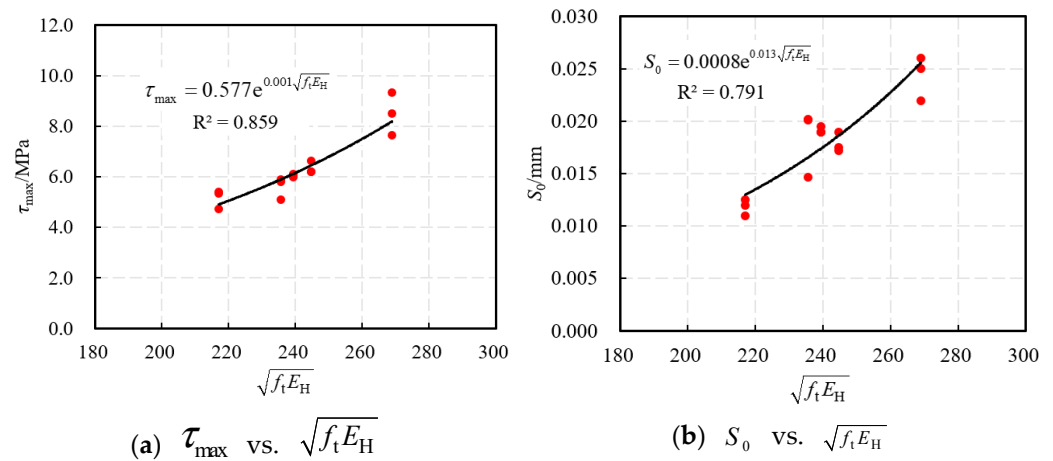
From Table 4, it can be seen that the bond-slip curve parameters are more significantly affected by the HTRCS material properties and concrete strength. Considering the dimensionless design,  $\sqrt{f_t E_H}$  is the independent variable, and  $\tau_{max}$  and  $S_0$  are the dependent variables. Figure 10 illustrates the regression analysis and gives Equations (5) and (6) with their  $R^2$  as 0.859 and 0.791, respectively.

$$\tau_{max} = 0.577e^{0.001\sqrt{f_t E_H}} \quad (6)$$

$$S_0 = 0.0008e^{0.013\sqrt{f_t E_H}} \quad (7)$$

**Table 4.** Parameters of bond-slip curve.

Specimens	$\tau_{\max}$	$S_0$	$f_t/\text{MPa}$	$E_H/\text{MPa}$
DS1-1	5.42	0.0125	2.35	$2.0 \times 10^4$
DS1-2	5.35	0.0110	2.35	$2.0 \times 10^4$
DS1-3	4.72	0.0120	2.35	$2.0 \times 10^4$
DS2-1	5.10	0.0201	2.77	$2.0 \times 10^4$
DS2-2	5.91	0.0134	2.77	$2.0 \times 10^4$
DS2-3	5.8	0.0200	2.77	$2.0 \times 10^4$
DS3-1	6.65	0.0172	2.98	$2.0 \times 10^4$
DS3-2	6.22	0.0175	2.98	$2.0 \times 10^4$
DS3-3	6.21	0.0190	2.98	$2.0 \times 10^4$
DS4-1	8.50	0.0260	2.98	$2.4 \times 10^4$
DS4-2	9.33	0.0197	2.98	$2.4 \times 10^4$
DS4-3	7.64	0.0250	2.98	$2.4 \times 10^4$
DS5-1	5.98	0.0195	2.98	$1.9 \times 10^4$
DS5-2	6.09	0.0287	2.98	$1.9 \times 10^4$
DS5-3	6.10	0.0190	2.98	$1.9 \times 10^4$

**Figure 10.** Regression analysis.

As can be seen from Figure 10,  $\tau_{\max}$  and  $S_0$  are shown to be positively correlated with  $\sqrt{f_t E_H}$ , indicating that the higher the concrete strength and the elastic modulus of HTRCS, the better the bond behavior between the interface of HTRCS and concrete. The high  $R^2$  values of the equation established by regression analysis indicate that the bond-slip model of HTRCS and concrete established in this paper has good accuracy. Furthermore, an accurate bond-slip model is also required for the establishment of an interfacial bearing capacity formula.

#### 4.2. Bearing Capacity Formula

There are few studies on the load bearing capacity formulae at the interface between HTRCS and concrete. However, HTRCS composite material can be regarded as a sheet, and its bond to concrete can be referred to as the bond between an FRP sheet and concrete. Lu [29] and Neubauer [30] have conducted a series of tests and an extensive finite element study on the bond between the sheet and concrete, and they concluded that the load bearing capacity equation is mainly affected by factors such as the elastic modulus of the bonding material, thickness, bond length, and concrete strength. With reference to the relevant literature, for the interface bonding between HTRCS and concrete, the following bearing capacity calculation formula is proposed:

$$P_u = k\beta_w\beta_l b_H \sqrt{2E_H t_H f_t} \quad (8)$$

$$\beta_w = \sqrt{\frac{2.25 - b_f/b_c}{1.25 + b_f/b_c}} \quad (9)$$

$$\beta_l = \frac{L}{L_e} \left(2 - \frac{L}{L_e}\right), L < L_e \quad (10)$$

$$\beta_l = 1, L \geq L_e \quad (11)$$

$$L_e = 1.33 \frac{\sqrt{E_f t_f}}{f_t} \quad (12)$$

where  $P_u$  is the interface bearing capacity;  $k$  is the interface bonding coefficient;  $\beta_w$  is the width influence coefficient;  $\beta_l$  is the anchorage length coefficient;  $b_H$  is the width of the HTRCS;  $b_c$  is the width of the concrete;  $L$  is the actual adhesive length;  $L_e$  is the effective bonding length; and  $f_t$  is the tensile strength of the concrete.

In the above established formula for calculating the interfacial bond bearing capacity of HTRCS composite material and concrete, the interfacial bond coefficient  $k$  is unknown. Through regression analysis,  $k = 0.286$  is obtained, and the square of the correlation coefficient is found to be 0.857, as shown in Figure 11.

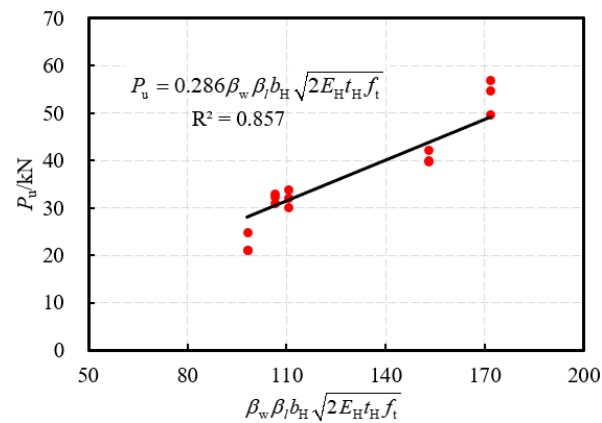


**Figure 11.** Regression analysis of  $k$ .

Currently, there are fewer studies on HTRCS composites, and even fewer on the interfacial bonding properties between HTRCS and concrete, so this paper is only based on experimental data to validate the bearing capacity equations established above. Table 5 shows the comparison between the calculated and test values for each specimen, SD is standard deviation, and COV is coefficient of variation. The prediction accuracy of the proposed load-bearing capacity formula is good, and the average value of the ratio of test values to calculated values is 0.978; the SD is 0.115 and the COV is 0.118. Therefore, the proposed formulae can accurately predict the interfacial bearing capacity between HTRCS and concrete. However, the applicability of the proposed prediction model is limited. The effects of factors such as interfacial bond length, the width ratio of concrete to composite layers, and interfacial cleanliness on interfacial bond behavior have not been tested and analyzed in depth. Therefore, in future studies, it is necessary to further explore the modification of the formulae by the key parameters and provide suggestions for engineers in practical applications.

**Table 5.** Comparison between test values and calculation values.

Specimens	$P_{u,exp}/kN$	$P_{u,cal}/kN$	$P_{u,exp}/P_{u,cal}$
DS1-1	21.18	28.03	0.76
DS1-2	24.75	28.03	0.88
DS1-3	21.16	28.03	0.75
DS2-1	32.92	30.42	1.08
DS2-2	32.31	30.42	1.06
DS2-3	30.98	30.42	1.02
DS3-1	32.05	31.59	1.01
DS3-2	33.86	31.59	1.07
DS3-3	30.16	31.59	0.95
DS4-1	56.89	49.12	1.16
DS4-2	54.73	49.12	1.11
DS4-3	49.64	49.12	1.01
DS5-1	40.05	43.72	0.92
DS5-2	42.14	43.72	0.96
DS5-3	39.88	43.72	0.91
	Average		0.978
	SD		0.115
	COV		0.118

## 5. Conclusions

In this paper, the interfacial bond behavior of HTRCS material and concrete is discussed through a double shear test. The main parameters involve concrete strength and HTRCS material properties. The failure modes, force-displacement relationship, and strain distribution of specimens are analyzed. The bond-slip model and bearing capacity formula are proposed. The following conclusions are drawn:

- (1) The failure mode of DS1 specimens was partial debonding and fracture, and the rest of the specimens were the fracture of HTRCS. The bond between the wire mesh and the resin concrete was good, and there was no obvious slip.
- (2) The concrete strength and reinforcement ratios of HTRCS composites were positively correlated with interfacial adhesion properties. When the concrete strength was increased from C30 to C40 and C50, the ultimate load increased by 43.4% and 43.2%, respectively. The ultimate load capacity increased by 32.1% with the reinforcement ratio of HTRCS composites increasing from 1.05% to 1.83%.
- (3) The stress transfer effect is positively correlated with the concrete strength and reinforcement ratio of HTRCS; the higher the concrete strength and reinforcement ratio of HTRCS, the further the stress transfer distance.
- (4) A bond-slip model for the interface between HTRCS and concrete is proposed and corrected according to the test parameters. The calculation formula for the interface bearing capacity is also proposed, and the test values are in good agreement with the calculated values, with an average value of 0.978.

**Author Contributions:** Conceptualization, Q.Y. and Y.Y.; investigation, A.L.; data curation, A.L.; writing—original draft preparation, Q.Y. and Y.R.; writing—review and editing, Q.Y. and Y.R.; visualization, A.L.; supervision, Y.Y.; project administration, Y.Y.; funding acquisition, Y.Y. All authors have read and agreed to the published version of the manuscript.

**Funding:** This work was supported by the Science and Technology Project of Sichuan Province (Grant No. 2018RZ0102).

**Data Availability Statement:** Data are contained within the article.

**Conflicts of Interest:** Qu Yu and Yongqing Yang were employed by the company Sichuan Jiaoda Engineering Detection & Consulting Co., Ltd. The remaining authors declare that the research was conducted in the absence of any commercial or financial relationships that could be construed as a potential conflict of interest.

## References

1. Guo, R.; Ren, Y.; Li, M.; Hu, P.; Du, M.; Zhang, R. Experimental study on flexural shear strengthening effect on low-strength RC beams by using FRP grid and ECC. *Eng. Struct.* **2021**, *227*, 111434. [[CrossRef](#)]
2. Yang, X.; Gao, W.-Y.; Dai, J.-G.; Lu, Z.-D.; Yu, K.-Q. Flexural strengthening of RC beams with CFRP grid-reinforced ECC matrix. *Compos. Struct.* **2018**, *189*, 9–26. [[CrossRef](#)]
3. Yu, R.; Xia, M.; Yi, P.; Guo, S.; Guo, R. Study on the uniaxial tensile behavior of an FRP grid-ECC composite layer. *Case Stud. Constr. Mater.* **2024**, *20*, e02909.
4. Zhou, Y.W.; Guo, M.H.; Sui, L.L.; Xiong, F.; Hu, B.; Huang, Z.; Yun, Y. Shear strength components of adjustable hybrid bonded CFRP shear-strengthened RC beams. *Compos. Part B Eng.* **2018**, *163*, 36–51. [[CrossRef](#)]
5. Rakgate, S.M.; Dundu, M. Strength and ductility of simple supported R/C beams retrofitted with steel plates of different width-to-thickness ratios. *Eng. Struct.* **2018**, *40*, 192–202. [[CrossRef](#)]
6. Torabian, A.; Isufi, B.; Mostofinejad, D.; Ramos, A.P. Behavior of thin lightly reinforced flat slabs under concentric loading. *Eng. Struct.* **2019**, *196*, 109327. [[CrossRef](#)]
7. Huixiang, M.; Zhigang, L.; Zhang, Y.; Haoran, X. Research on the Bearing Capacity of the Cross Section of Reinforced Concrete Beams Strengthened with Increasing Section Method Considering the Effect of the Second Loading. *Adv. Res.* **2015**, *5*, 1–9. [[CrossRef](#)]
8. Shakir, Q.M.; Abdlsaheb, S.D. Rehabilitation of partially damaged high strength RC corbels by EB FRP composites and NSM steel bars. *Structures* **2022**, *38*, 652–671. [[CrossRef](#)]
9. Shakir, Q.M.; Abdlsaheb, S.D. Strengthening of the self-compacted reinforced concrete corbels using NSM steel bars and CFRP sheets techniques. *J. Eng. Sci. Technol.* **2022**, *17*, 1764–1780.
10. Singh, S.; Vummadisetti, S.; Chawla, H. Influence of curing on the mechanical performance of FRP laminates. *J. Build. Eng.* **2018**, *16*, 1–19. [[CrossRef](#)]
11. Li, Y.Y.; Guo, B.; Liu, J. Research on reinforced concrete beam enlarged cross section method experiment and finite element simulation. *Appl. Mech. Mater* **2014**, *638*, 208–213. [[CrossRef](#)]
12. De Lorenzis, L.; Teng, J.G. Near-surface mounted FRP reinforcement: An emerging technique for strengthening structures. *Compos. Part B Eng.* **2007**, *38*, 119–143. [[CrossRef](#)]
13. Zhang, S.S.; Yu, T.; Chen, G.M. Reinforced concrete beams strengthened in flexure with near-surface mounted (NSM) CFRP strips: Current status and research needs. *Compos. Part B Eng.* **2017**, *131*, 30–42. [[CrossRef](#)]
14. Liu, Z.-Q.; Guo, Z.-X.; Ye, Y. Flexural behaviour of RC beams strengthened with prestressed steel wire ropes polymer mortar composite. *J. Asian Arch. Build. Eng.* **2021**, *21*, 48–65. [[CrossRef](#)]
15. Emar, M.; Rizk, M.; Mohamed, H.; Zaghlal, M. Enhancement of circular RC columns using steel mesh as internal or external confinement under the influence of axial compression loading. *Frat. Integrità Strutt.* **2021**, *15*, 86–104. [[CrossRef](#)]
16. Marthong, C. Compressive behavior of galvanized steel wire mesh (GSWM) strengthened RC short column of varying shapes. *Struct. Monit. Maint.* **2020**, *7*, 215–231.
17. Zhang, K.; Xuan, J.; Shen, X.; Xue, X. Investigating the Flexural Properties of Reinforced Concrete T-Beams Strengthened with High-Strength Steel Wire Mesh and Polyurethane Cement. *J. Bridge Eng.* **2024**, *29*, 86–104. [[CrossRef](#)]
18. Zhao, H. Axial compressive behaviour of concrete strengthened with steel rings, wire mesh and modified high strength mortar (MHSM). *Constr. Build. Mater.* **2020**, *250*, 118938. [[CrossRef](#)]
19. Yuan, F.; Chen, M.; Pan, J. Flexural strengthening of reinforced concrete beams with high-strength steel wire and engineered cementitious composites. *Constr. Build. Mater.* **2020**, *254*, 119284. [[CrossRef](#)]
20. Wang, X.; Yang, G.; Qian, W.; Li, K.; Zhu, J. Tensile behavior of high-strength stainless steel wire rope (HSSSWR)-reinforced ECC. *Int. J. Concr. Struct. Mater.* **2021**, *15*, 43. [[CrossRef](#)]
21. Zheng, Y.-Z.; Wang, W.-W.; Brigham, J.C. Flexural behaviour of reinforced concrete beams strengthened with a composite reinforcement layer: BFRP grid and ECC. *Constr. Build. Mater.* **2016**, *115*, 424–437. [[CrossRef](#)]
22. Zheng, Y.-Z.; Wang, W.-W.; Mosalam, K.M.; Fang, Q.; Chen, L.; Zhu, Z.-F. Experimental investigation and numerical analysis of RC beams shear strengthened with FRP/ECC composite layer. *Compos. Struct.* **2020**, *246*, 112436. [[CrossRef](#)]
23. Yan, M. *Concrete with Steel High Toughness Resin Wire Mesh and the Reinforcement Theoretical Research on Prestressed Concrete Simply Supported Plate Beam Bridge*; Southwest Jiaotong University: Chengdu, China, 2015.
24. Ren, Y.; Gao, Z.; Xia, M.; Guo, R. Study on bonding behavior of FRP grid-ECC composite layer and concrete with quantitative interface treatment. *Eng. Struct.* **2023**, *294*, 116768. [[CrossRef](#)]
25. GB 50010-2010; Code for Design of Concrete Structures. China Architecture & Building Press: Beijing, China, 2010.
26. Dai, J.G.; Ueda, T.; Sato, Y. Development of the nonlinear bond stress-slip model of fiber reinforced plastics sheet-concrete interfaces with a simple method. *J. Compos. Constr.* **2005**, *9*, 52–62. [[CrossRef](#)]
27. Ferracuti, B.; Savoia, M.; Mazzotti, C. Interface law for FRP—Concrete delamination. *Compos. Struct.* **2007**, *80*, 523–531. [[CrossRef](#)]
28. Lu, X.Z.; Teng, J.G.; Ye, L.P.; Jiang, J.J. Bond-slip models for FRP sheets/plates bonded to concrete. *Eng. Struct.* **2005**, *27*, 920–937. [[CrossRef](#)]

29. Lu, X.Z. *Studies on FRP-Concrete Interface*; Tsinghua University: Beijing, China, 2005.
30. Neubauer, U.; Rostasy, F.S. Design aspects of concrete structures strengthened with externally bonded CFRP plates. In Proceedings of the 7th International Conference on Structural Faults and Repair, Edinburgh, UK, 8 July 1997; ECS Publications: Edinburgh, UK, 1997; Volume 2, pp. 109–118.

**Disclaimer/Publisher's Note:** The statements, opinions and data contained in all publications are solely those of the individual author(s) and contributor(s) and not of MDPI and/or the editor(s). MDPI and/or the editor(s) disclaim responsibility for any injury to people or property resulting from any ideas, methods, instructions or products referred to in the content.